Vibrational relaxation of highly excited toluene

Beatriz M. Toselli,[a] Jerrell D. Brenner, Murthy L. Yerram,[b] William E. Chin,[c] Keith D. King,[d] and John R. Barker[e]
The Department of Atmospheric, Oceanic, and Space Sciences, Space Physics Research Laboratory, The University of Michigan, Ann Arbor, Michigan 48109-2143

(Received 1 March 1991; accepted 25 March 1991)

The collisional loss of vibrational energy from gas-phase toluene, pumped by a pulsed KrF laser operating at 248 nm, has been observed by monitoring the time-resolved infrared fluorescence from the C–H stretch modes near 3.3 μm. The fragmentation quantum yield of toluene pumped at 248 nm was determined experimentally to be $\sim 6\%$. Energy transfer data were obtained for 20 collider gases, including unexcited toluene, and analyzed by an improved inversion technique that converts the fluorescence intensity to the bulk average energy, from which is extracted $\langle\langle \Delta E \rangle\rangle$, the bulk average amount of energy transferred per collision. Comparisons are presented of these results with similar studies of benzene and azulene, and with the time-resolved ultraviolet absorption study of toluene carried out by Hippler *et al.* [J. Chem. Phys. **78**, 6709 (1983)]. The present results show $\langle\langle \Delta E \rangle\rangle$ to be nearly directly proportional to the vibrational energy of the excited toluene from 5000 to 25 000 cm^{-1}. For many of the colliders at higher energies, the energy dependence of $\langle\langle \Delta E \rangle\rangle$ is somewhat reduced. A simple method is described for obtaining good estimates of $\langle \Delta E \rangle_d$ (the energy transferred per collision in deactivating collisions) by carrying out an appropriate least-squares analysis of the $\langle\langle \Delta E \rangle\rangle$ data. The values of $\langle \Delta E \rangle_d$ are then used in master-equation calculations to investigate possible contributions from "supercollisions" (in which surprisingly large amounts of energy are transferred) in the deactivation of toluene.

I. INTRODUCTION

The vibrational relaxation of highly excited molecules has a large influence on many chemical processes and it has been investigated by a variety of experimental and theoretical methods. Traditionally, energy transfer has been investigated in unimolecular reaction systems,[1] but physical techniques, which can be used below the dissociation energy, have proved to be very useful in measurements of $\langle\langle \Delta E \rangle\rangle$, the bulk average amount of energy transferred per collision. Direct experimental results on $\langle\langle \Delta E \rangle\rangle$ are available for excited triatomic and large polyatomic molecules over a wide range of vibrational energy and temperature. Most of the studies have been carried out using time-resolved infrared fluorescence (IRF) or ultraviolet absorption (UVA). The IRF technique has been used to measure the collisional deactivation of azulene,[2] 1,1,2-trifluoroethane,[3] benzene,[4] and several of its derivatives.[5] The UVA technique has been used to study energy transfer in several large polyatomic molecules,[6,7] CF_3I,[8] and the triatomics SO_2 (Ref. 9) and CS_2.[10] In addition, techniques based on photothermal processes have been employed for energy-transfer studies.[11-14] Techniques developed recently by Luther and co-workers[15] and by Weisman and co-workers[16] promise to provide information that is even more detailed.

The present work is part of a series of investigations of benzene derivatives, which are large molecules with high densities of states, but are small enough to provide practical tests of theoretical calculations. Theoretical descriptions of large-molecule energy transfer have lagged behind the experimental measurements, although some progress is being made. Several theoretical models have been developed for large molecule energy transfer, including models originally developed for small molecules and then extended to larger species. Some of these models, such as the Schwartz–Slawsky–Herzfeld theory[17] as extended by Tanczos[18] and corrected by Yardley, are discussed by Yardley.[19] Later, statistical models and statistical dynamical models were developed to explain experimental data on $\langle\langle \Delta E \rangle\rangle$.[1,20] Of special note are the impulsive ergodic collision theory, developed by Schranz and Nordholm,[21] the model described by Sceats,[22] and the approach taken by Gilbert[23] and Lim and Gilbert,[24] who have described the biased random-walk model, which has only been applied to monatomic colliders thus far. One avenue for theoretical development is the use of classical trajectory calculations, although they suffer from fundamental defects, as described elsewhere,[25] and they depend on detailed potential-energy surfaces, which are largely unknown. Nonetheless, trajectory calculations carried out by Lim and Gilbert for azulene[26] and by Schatz and co-workers for CS_2 (Ref. 27) seem to be quite successful in describing major qualitative features of collisional energy transfer.

Toluene has been the subject of previous energy transfer studies. Hippler and co-workers[6(a)-6(c)] used the UVA technique to follow the collisional deactivation of highly excited toluene produced from the photoisomerization of cycloheptatriene. In that experiment the toluene molecules were prepared with 52 000 cm^{-1} of vibrational excitation after irra-

[a] Present address: Physical Chemistry Branch, Chalk River Laboratories, Atomic Energy of Canada, Chalk River, Ontario, Canada K01 1J0.
[b] Present address: Department of Chemical Engineering and Materials Science, University of Minnesota, Minneapolis, MN 55455.
[c] Present address: Department of Physics, Denison University, Granville, OH 43023.
[d] On Sabbatical leave from The Department of Chemical Engineering, The University of Adelaide, G.P.O. Box 498, Adelaide, South Australia 5001.
[e] Also at Department of Chemistry.

 0021-9606/91/130176-13$03.00

diation of the cycloheptatriene, which undergoes fast internal conversion and subsequent molecular isomerization to form the highly excited toluene. At this high energy the toluene molecule can further dissociate into benzyl radicals and H atoms ($E_0 = 30\,180\ \text{cm}^{-1}$), but this decomposition can be minimized by efficient competition of collisions. Hippler and co-workers carried out a very complete study, investigating the deactivation of the excited toluene by about 60 different collider gases. Their results will be discussed further and will be compared with the present work in Sec. IV.

Luther and co-workers[15] have developed a multiphoton ionization method (termed "kinetically controlled selective ionization:" KCSI) that promises to give detailed information about the time-dependent population distributions that occur during the vibrational deactivation of large molecules. Currently, the collisional deactivation of toluene produced by the photoisomerization of cycloheptatriene is being investigated by this technique and only preliminary results have been published.[15] By varying the delay time between the pump laser and the multiphoton ionization probe laser, the time evolution of the population distribution at selected energies can be monitored during the relaxation. An advantage of this technique is that the KCSI signal gives information about the higher moments of the population distribution, in addition to $\langle\langle \Delta E \rangle\rangle$. A disadvantage of the technique is that the accessible energy window is quite low ($< 10\,000\ \text{cm}^{-1}$) and the photophysics of the multiphoton ionization must be characterized fully.

An important result of the KCSI experiments on toluene is that "supercollisions" make a contribution.[15] Supercollisions are collisions in which an unusually large amount of energy is transferred. The existence of supercollisions was inferred by Oref and co-workers from experiments with cyclobutene excited by large molecule colliders,[28] and the KCSI experiments indicate they are also present in the deactivation of toluene. Recent classical trajectory calculations provide supporting evidence.[29] The presence of supercollisions can strongly affect the time-dependent population distributions produced in collisional deactivation and they may also affect measurements of $\langle\langle \Delta E \rangle\rangle$.

In the present work, the IRF technique is used to monitor the collisional deactivation of highly vibrationally excited toluene pumped with a KrF excimer laser at 248 nm. This study is part of a larger effort (which began with investigations of azulene and benzene) to compile an experimental database that will aid in understanding how different molecular properties affect the energy transfer process. An important aspect of this effort is to develop methods for the extraction of the energy-transfer parameters from the measured IRF decay, while minimizing systematic errors due to the analysis method. Moreover, careful attention is given to the evaluation of the statistical errors in order to facilitate valid comparisons with other experimental and theoretical studies. An added feature of the present work is the description of a simple, reasonably accurate method for estimating $\langle \Delta E \rangle_d$, the average energy transferred in *deactivating* collisions, which is often the most useful energy transfer parameter for implementing master-equation calculations. Finally, the possible contributions of supercollisions to the present results are investigated through the use of master-equation calculations.

II. EXPERIMENT

The collisional relaxation of toluene was monitored with the IRF technique, which has been described elsewhere in detail.[2,4] Basically, a KrF excimer laser (248 nm) irradiated the gas-phase species in a 30 cm long, 4.5 cm diam Pyrex cell. Laser-beam transmittance measurements carried out with a Scientech volume-absorbing calorimetric power meter gave an absorption cross section of $(3.7 \pm 0.2) \times 10^{-19}\ \text{cm}^2$ (base e) at 248 nm for toluene, very similar to the value obtained previously for benzene.[4] The average laser fluence employed in the present measurements was $\sim 25\ \text{mJ cm}^{-2}$, such that $\sim 0.5\%$ of the molecules in the laser beam were excited. This laser fluence may be high enough to produce multiphoton ionization of a small fraction of the toluene, as in benzene,[30] but no indications of this process were observed. The C–H stretch IRF emission near 3.3 μm was viewed through a quartz side window by a 3 mm diam InSb (77 K) photovoltaic detector (Infrared Associates) equipped with a matched preamplifier and an interference filter. The signals were further amplified with a Tektronix AM 502 ac-coupled amplifier and averaged with a LeCroy 9400 digital oscilloscope for ~ 5000 pulses, in order to achieve good signal/noise ratios in each experiment. The signal was further analyzed after transfer to a Macintosh personal computer. The IRF signal time response was limited by the $\sim 5\ \mu$s rise time of the infrared detector/preamplifier, as described previously.[4]

Toluene (Aldrich) was degassed prior to use. Flowing conditions were employed for pure toluene decay measurements and pressures in the cell were varied from 10 to 50 mTorr (at pressures lower than 10 mTorr, diffusion of the excited species and deactivation on the cell walls may introduce complications). Collider gas experiments were performed under static bulb conditions in mixtures containing 10 mTorr of toluene ("parent" gas) and up to about 800 mTorr of the collider. The collider gases were all research grade and were used without further purification. The gas samples were introduced into the cell through a fine-control needle valve and pressures were monitored with a 0–1 Torr capacitance manometer (MKS Baratron model 227).

A small pressure decrease was observed while irradiating pure toluene (10–50 mTorr) under static bulb conditions, indicating the presence of photolytic reactions. Some polymeric deposition on the walls has been reported in the literature for higher pressure conditions; in our experiments (involving much lower pressure) a brown film developed on the windows at the sites of entry and exit of the laser beam. The possible formation of products was investigated in Ref. 31, where it was concluded that the yield of CH_4 and H_2 or C_2H_6 was negligible. The absence of bibenzyl in that study suggested that if benzyl radical were formed, the only significant reaction was the recombination to re-form toluene. In order to determine the possible effects of toluene photodecomposition in the static cell experiments [the threshold en-

ergy to produce the benzyl radical and H atom is $\sim 30\,180$ cm^{-1} (Ref. 32)], we used a modulated molecular-beam mass spectrometer to search for photoproducts, as described previously.[4] The quantum yield for toluene loss was found to be $6 \pm 2\%$, and the only gas-phase product detected was H_2. This result is consistent with the formation of benzyl radicals and hydrogen atoms, which can react to produce H_2 and bibenzyl, which has too low a vapor pressure at room temperature to be detected in our experiments; this set of products can explain both the small pressure decrease observed and the film deposited on the windows.

The effect of the toluene photodecomposition on the IRF measurements is probably quite small, because the $\sim 10\,000$ cm^{-1} energy remaining after photodissociation must be partitioned between the hydrogen atom and the benzyl free radical. Benzyl is likely to emit IRF near 3.3 μm and it may contribute to the observed signal. However, with $\leqslant 10\,000$ cm^{-1}, the initial fluorescence intensity of each benzyl radical will be $\leqslant 6\%$ of that of each excited toluene molecule, which contains $\sim 40\,000$ cm^{-1}. This small relative intensity, coupled with the low quantum yield for benzyl radical formation, will produce very little contribution by excited benzyl to the observed IRF signals.

III. TOLUENE PHOTOPHYSICS

In the present experiments toluene was excited at 248 nm to the S_1 state, which, as described below, subsequently undergoes radiationless transitions to form highly vibrationally excited molecules in the ground state (S_0). As mentioned in the preceding section, about 6% of the toluene also is lost through photodissociation. A fundamental requirement of the IRF experiment is that the rate of internal conversion (IC) or intersystem crossing (ISC) to the ground state in the surviving molecules must be rapid compared to collisional deactivation and infrared fluorescence. Therefore it is important to know the rates of the radiationless processes and the amount of energy that is lost by fluorescence from the excited S_1 state.

In excited toluene, conversion to the electronic ground state apparently occurs, as in benzene, through two successive ISC steps ($S_1 \rightarrow T_1 \rightarrow S_0$), and direct IC to the ground state is not important.[33] Much information is available about the spectroscopy and decay mechanisms of the first excited singlet states of aromatics, but less information is available concerning the low-lying triplets. Lifetimes of many S_1 levels at energies near the origin are known,[34] mostly determined by fluorescence lifetime measurements. Jacon *et al.*[35] studied the fluorescence decay times and quantum yields for isolated toluene molecules as a function of energy and wavelength. They found that the rate of nonradiative transitions from S_1 increases rapidly with energy: at 248 nm this rate is $\sim 3.3 \times 10^7$ s^{-1} and the fluorescence quantum yield is 0.09. Unfortunately, there are no direct measurements of the rate constant for $S_1 \rightarrow T_1$ ISC at an energy corresponding to 248 nm, but the rate constant for ISC is 8.5×10^6 s^{-1} at 37 500 cm^{-1},[33] and this value increases with the excitation energy; furthermore, it was found that IC can be neglected, because the quantum yields for fluorescence and for ISC account for 94% of the decay from the S_1 state. According to Burton and Noyes the same mechanism is likely operating at 40 300 cm^{-1} (248 nm). Thus, in the present experiments, the $S_1 \rightarrow T_1$ ISC is the dominant deactivation process of the S_1 state and its rate is probably $\sim 3 \times 10^7$ s^{-1}.

There are three measurements under collision free conditions of the T_1 triplet lifetime of toluene,[33,36,37] and these studies at the same energy reveal some minor discrepancies. For example, at $E(\text{vib},T_1) = 9370$ cm^{-1}, Luther and coworkers reported a value of $k_T = 3.4 \times 10^5$ s^{-1}, which is $\sim 30\%$ lower than the extrapolated value from Dietz, Duncan, and Smalley;[33] the latter measurement was reported to be twice as large as the value from Ref. 36. Notwithstanding these relatively small differences, a major concern of all these studies has been to explain the energy dependence of the radiationless decay rates. The $T_1 \rightarrow S_0$ ISC in some aromatics, including benzene and toluene, exhibits a very strong increase in rate within the first 1000–2000 cm^{-1} followed by a much more gradual increase (almost no energy dependence), a region termed the "saturation range." In the present experiments ($\sim 11\,500$ cm^{-1} of vibrational energy in the triplet state), the triplet state decay rate is $k_T \approx 10^6$ s^{-1}.[36]

Thus, we conclude that $\sim 90\%$ of the toluene molecules that do not decompose are found in highly vibrationally excited states of S_0 after ~ 1 μs, or less; the remaining $\sim 10\%$ are lost from view due to electronic fluorescence and do not participate in IRF emission.

IV. RESULTS AND DISCUSSION

A. Inversion of IRF data to obtain $\langle\langle E\rangle\rangle_{inv}$ and $\langle\langle \Delta E\rangle\rangle_{inv}$

A typical fluorescence decay curve obtained for pure toluene at 20 mTorr is shown in Fig. 1; the decay curves for other collider gases were similar, but had lower signal/noise (S/N) ratios and the decays occurred on different time scales. Due to the limited time response of the infrared detector, the intensity at $t = 0$ was not observed directly, but was obtained by back-extrapolation of a function fitted to the data obtained after 7 μs. As in previous experimental work,[2,4] these IRF decay curves, although approximately exponential, are better fitted to nonexponential empirical functions using nonlinear least squares. The Marquardt non-

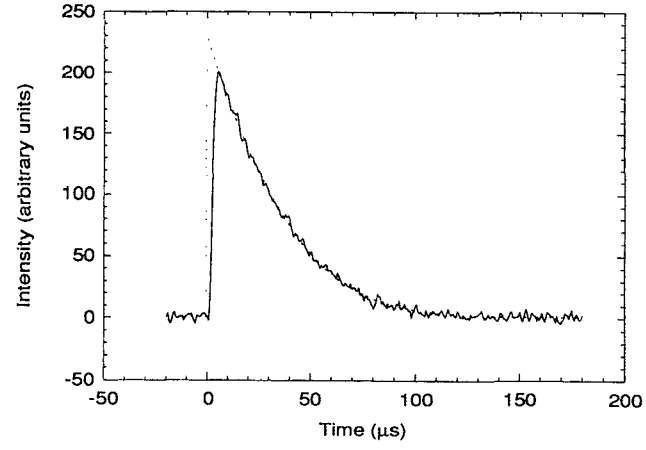

FIG. 1. C–H stretch IRF fluorescence decay. Conditions: 248 nm excitation, 20 mTorr toluene (flowing system).

linear least-squares algorithm[38] was used to obtain numerical fits to the following empirical function:

$$\langle\langle I(t)\rangle\rangle = A\exp(-k^I t + b^I t^2) + B, \quad (1)$$

where k^I and b^I are fitted parameters which depend on collider gas pressures (see below). This expression was used to obtain a smooth empirical fit to the experimental data and to extrapolate the intensity to $t = 0$.

In order to relate the observed IRF signal to the vibrational energy content of the excited toluene, the following theoretical expression[2,4] (originally from Durana and McDonald[39]) was used:

$$I(E) = \frac{N_{ex}}{\rho_s(E)} \sum_{i=1}^{\text{modes}} h\nu_i A_i^{1,0} \sum_{v_i=1}^{v_{max}} v_i \rho_{s-1}(E - v_i h\nu_i). \quad (2a)$$

Here, N_{ex} is the number of vibrationally excited molecules, $A_i^{1,0}$ is the Einstein coefficient for spontaneous emission for the $0 \leftarrow 1$ transition of mode i, v_i is its quantum number, $h\nu_i$ is the energy of the emitted photon, and $\rho_s(E)$ and $\rho_{s-1}(E - v_i h\nu_i)$ are, respectively, the density of states for all s oscillators at energy E and that for the $s-1$ modes, omitting the emitting mode and the energy contained in it. The summations are carried out for all vibrational modes that emit in the wavelength range observed and for all vibrational levels of each mode permitted by conservation of energy.

Because the vibrational frequencies of the C–H stretching modes are found in a narrow range of energy (3000 ± 60 cm^{-1}) and the absolute intensity is not used in the data analysis, the number of excited molecules, the photon energies, and the Einstein coefficients can be combined in an undetermined constant term, and a relative intensity, $I'(E)$, can be defined, which only involves densities of states and which is directly proportional to the average energy residing in the C–H stretch modes,

$$I'(E) = \frac{1}{\rho_s(E)} \sum_{i=1}^{\text{modes}} \sum_{v_i=1}^{v_{max}} v_i \rho_{s-1}(E - v_i h\nu_i). \quad (2b)$$

A vibrational assignment[40] for toluene was used to obtain the densities of states, which were evaluated using the Stein and Rabinovitch implementation[41] of the Beyer–Swinehart algorithm[42] for exact counts of states, as modified by Astholz, Troe, and Wieters[43] for free rotors.

To convert the observed intensity decays to energy decays, knowledge of the initial energy is exploited to scale the experimental data so that the initial intensity corresponds to that calculated according to Eq. (2b): $I'(t=0) = 0.177$. The initial energy is taken to be the sum of the photon energy ($\sim 40\,300\ cm^{-1}$) and the average thermal energy of toluene at 300 K ($\sim 700\ cm^{-1}$). The scaled experimental intensity data, or its least-squares fit, can then be "inverted" to give the corresponding energy. To facilitate this process, values of $I'(E)$ were calculated for the energy range from 5000 to 45 000 cm^{-1} and the results least-squares fitted to give the following expression:

$$\ln E = 11.9241 + 0.897\,03 \ln I' + 0.093\,16(\ln I')^2 + 0.006\,396(\ln I')^3 + 0.000\,226(\ln I')^4, \quad (3)$$

where

$$5000\ cm^{-1} \leqslant E < 45\,000\ cm^{-1}.$$

To obtain the energy transfer parameters, the experimental intensity decays must be converted to energy decays and subsequently differentiated to obtain $\langle\langle \Delta E \rangle\rangle$, the average energy-transfer step size,

$$\frac{d}{dt}\langle\langle E\rangle\rangle = k_{LJ} N \langle\langle \Delta E\rangle\rangle, \quad (4a)$$

$$\frac{d}{dZ}\langle\langle E\rangle\rangle = \langle\langle \Delta E\rangle\rangle. \quad (4b)$$

Here, the double angular brackets[44] denote bulk averages of vibrational energy and energy-transfer step sizes, k_{LJ} is the Lennard-Jones collision rate constant, N is the number density of collider, and $Z(= k_{LJ} N t)$ is the number of collisions. It is important to note that the product $k_{LJ}\langle\langle \Delta E\rangle\rangle$ appears in Eq. (4), and not the individual terms; the separation of this product into separate terms is arbitrary and is done for historical reasons and for convenience. In comparisons with other work, it may be necessary to adjust the values for $\langle\langle \Delta E\rangle\rangle$ to compensate for different choices of k_{LJ}. In the present work, values of k_{LJ} were determined in the same manner and with the same Lennard-Jones parameters as in Ref. 6(b) in order that direct comparisons can be made easily; the numerical values are collected in Table I.

Note that the population distributions evolve with time and thus both $\langle\langle E\rangle\rangle$ and $\langle\langle \Delta E\rangle\rangle$ are time dependent. Since both $\langle\langle E(t)\rangle\rangle$ and $\langle\langle \Delta E(t)\rangle\rangle$ are determined for the same instant of time from the experimental data, $\langle\langle \Delta E\rangle\rangle$ can be expressed as a function of $\langle\langle E\rangle\rangle$. To emphasize that the bulk average energies and step sizes were obtained from experimental data according to the inversion methods described in this section, the subscript "inv" is added: $\langle\langle E\rangle\rangle_{inv}$ and $\langle\langle \Delta E\rangle\rangle_{inv}$.

For experiments involving collider gases it is necessary to account for the effects of self-collisions (toluene*–toluene), in addition to collisions of excited toluene with the collider gas. In the present work two different approaches were evaluated: methods *A* and *B*. Method *A* was used previously to extract energy-transfer parameters in experiments with benzene, where a full description of the method is presented.[4] Basically, method *A* is as follows: (a) each experimental decay curve is normalized according to laser pulse energy and absorber number density and the intensities were normalized so that the average intensity of all runs at $t = 0$ was equal to 0.177 (see above), but individual runs may differ; (b) it is assumed that the decay rate of the IRF signal is due to the linear combination of parent and collider contributions, i.e., a linear sum rule (LSR) is assumed for the parameters in Eq. (1): $k^I = k_p N_p + k_c N_c$ and $b^I = b_p N_p^2 + b_c N_c^2$, where k_i and b_i are constants and N_i represents the concentration of the parent or collider; (c) assuming the validity of the LSR, a least-squares fit gives empirical values for k_c, b_c, k_p, and b_p, and synthetic IRF decay curves are generated based on k_c and b_c in Eq. (1) (i.e., contributions from collisions with parent gas are neglected); (d) the full covariance matrix resulting from the nonlinear least-squares fit is assumed to be associated with

TABLE I. Collider gas data.

Collider	σ_{LJ} [a] (Å)	ϵ/K [a] (K)	$10^{10}k_{LJ}$ ($cm^3\,s^{-1}$)	$-\langle\langle\Delta E\rangle\rangle_{inv}$ [b,c] (cm^{-1})	C_1 (cm^{-1})	$\langle\Delta E\rangle_d$ [d] C_2	10^7C_3 ($1/cm^{-1}$)
C_7H_8	5.92	410	7.32	867 ± 18	46.2	0.0538	− 4.57
He	2.55	10	7.14	62 ± 1	28.6	0.007 84	− 1.00
Ne	2.82	32	4.26	77 ± 2	32.4	0.009 84	− 1.47
Ar	3.47	114	4.62	112 ± 3	36.1	0.008 98	− 0.323
Kr	3.66	178	4.15	110 ± 4	36.1	0.009 85	− 0.769
Xe	4.05	230	4.25	124 ± 6	44.1	0.009 54	− 0.0406
H_2	2.83	60	13.57	89 ± 3	29.1	0.010 66	− 1.49
D_2	2.73	69	9.69	103 ± 2	38.7	0.011 64	− 1.69
N_2	3.74	82	5.27	139 ± 4	39.3	0.0159	− 2.63
O_2	3.48	103	4.93	151 ± 3	35.4	0.0142	− 1.63
CO	3.70	105	5.44	163 ± 3	34.8	0.0144	− 1.47
CO_2	3.94	201	5.46	245 ± 6	37.4	0.0230	− 3.33
H_2O	2.71	506	7.13	364 ± 13	52.1	0.0323	− 5.05
D_2O	2.71	506	6.82	293 ± 8	70.4	0.017 97	− 0.691
CH_4	3.79	153	7.43	225 ± 6	47.1	0.0197	− 2.54
NH_3	2.90	558	7.80	285 ± 10	48.6	0.0213	− 1.94
SF_6	5.20	212	5.09	368 ± 4	46.9	0.0292	− 3.50
c–C_3H_6	4.63	299	6.86	576 ± 12	22.6	0.0473	− 7.01
C_3H_6	4.78	271	6.92	487 ± 12	38.7	0.0333	− 0.307
n–C_4H_{10}	5.40	307	7.15	619 ± 18	57.2	0.0403	− 3.51

[a] Lennard-Jones parameters (for collider gases) from Ref. 6(b).
[b] Uncertainties are ± 2σ statistical errors; possible systematic errors are not included.
[c] Evaluated at $\langle\langle E\rangle\rangle_{inv} = 24\,000\ cm^{-1}$.
[d] $\langle\Delta E(E)\rangle_d = C_1 + C_2E + C_3E^2$.

k_c and b_c (i.e., it is assumed that there is no uncertainty associated with contributions due to parent gas) in the subsequent propagation of errors analysis; (e) inversion of resulting predicted net decay curves through use of Eq. (3) gives $\langle\langle E(t)\rangle\rangle_{inv}$ and $\langle\langle\Delta E\rangle\rangle_{inv}$ for the toluene* + collider gas collisions; (f) propagation of errors is carried out using the full covariance matrix to obtain uncertainties in $\langle\langle E\rangle\rangle_{inv}$ and $\langle\langle\Delta E\rangle\rangle_{inv}$.

An example plot of $\langle\langle\Delta E\rangle\rangle_{inv}$ vs $\langle\langle E\rangle\rangle_{inv}$ and estimated uncertainties obtained using method *A* is shown in Fig. 2. One of the limitations of method *A* is apparent in the figure: the estimated uncertainty in $\langle\langle E\rangle\rangle_{inv}$ is much larger than expected at high energy, which corresponds to times early in the decay, when the energy is known best: at $t = 0$, there should be no uncertainty in $\langle\langle E\rangle\rangle_{inv}$. This overestimate of the uncertainty is due to the assumption that all sources of error reside in the IRF decay, even though significant errors are associated with laser power measurements and pressure measurements.

A second very important limitation of method *A* is that the assumed LSR may not be valid. A new approach, method *B*, has been developed in order to eliminate that assumption and to provide better estimates of uncertainty. In method *B*, the validity of LSR is not assumed and the total decay of the IRF signal is considered. The procedure is as follows: (a) every experimental decay curve is normalized individually so that its extrapolated intensity at $t = 0$ is $I_0 = 0.177$ (see above); (b) the least-squares fit of $\langle\langle I(t)\rangle\rangle$ vs time is inverted through use of Eqs. (3) and (4) to obtain $\langle\langle\Delta E\rangle\rangle_{inv}$ and $\langle\langle E\rangle\rangle_{inv}$ for the gas mixture; (c) for selected values of $\langle\langle E\rangle\rangle_{inv}$ (typically each 1000 cm^{-1}) curves are constructed of $\langle\langle\Delta E\rangle\rangle_{inv}$ vs F_c, the fraction of collisions that occur with the collider gas:

$$F_c = \frac{N_c k_{LJ}^c}{N_c k_{LJ}^c + N_p k_{LJ}^p}, \tag{5}$$

where k_{LJ}^i is the collision rate constant corresponding to collisions of excited toluene with collider gas ($i = c$), or parent ($i = p$). The next step is (d) to extrapolate to $\langle\langle\Delta E\rangle\rangle_{inv}$ at each energy to $F_c = 1.0$ to obtain $\langle\langle\Delta E\rangle\rangle_{inv}$ for collider, uncontaminated by the effects of parent–parent gas collisions; (e) propagation of errors is carried out to estimate the uncertainties in $\langle\langle E\rangle\rangle_{inv}$ and $\langle\langle\Delta E\rangle\rangle_{inv}$. Note that instead of collision fraction, ordinary mole fraction could have been used for the extrapolation to pure collider, but plots of

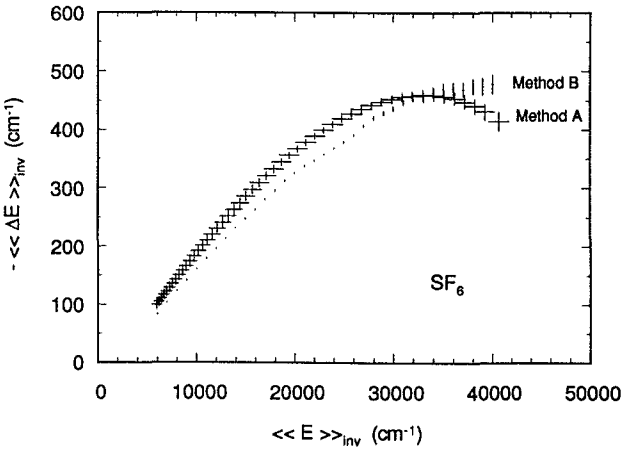

FIG. 2. $-\langle\langle\Delta E\rangle\rangle_{inv}$ vs $\langle\langle E\rangle\rangle_{inv}$ for toluene* deactivation by SF_6. Comparison of the results of two analysis methods applied to the same experimental data set (see text for details). Note the differences in estimated uncertainties.

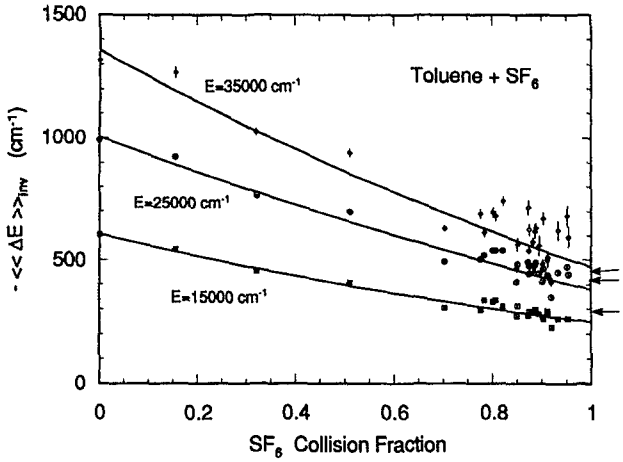

FIG. 3. – $\langle\langle \Delta E \rangle\rangle_{inv}$ vs collision fraction of SF_6. The arrows indicate values determined using method *A* (see text for details).

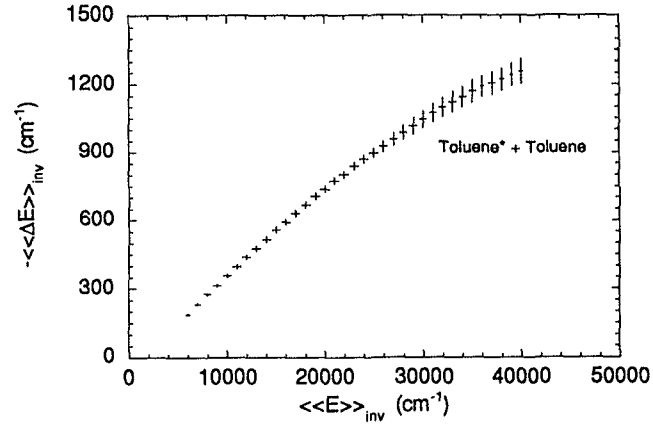

FIG. 4. – $\langle\langle \Delta E \rangle\rangle_{inv}$ vs $\langle\langle E \rangle\rangle_{inv}$ for toluene* deactivation by unexcited toluene.

$\langle\langle \Delta E \rangle\rangle_{inv}$ vs collision fraction are more nearly linear.

Figure 3 shows $\langle\langle \Delta E \rangle\rangle_{inv}$ as a function of F_c at selected average vibrational energies for the toluene*–SF_6 system using method *B*. Extrapolation to $F_c = 1$ gives $\langle\langle \Delta E \rangle\rangle_{inv}$ for toluene*–SF_6 collisions. This method is advantageous in that the contributions of toluene*–toluene collisions need not be artificially subtracted from the energy decay (as in method *A*, using the linear sum rule). Although Fig. 3 does not show large deviations from the LSR for this particular case, such deviations have been found to be significant for other collider gases.[5] The arrows at $F_c = 1$ in Fig. 3 show the values of $\langle\langle \Delta E \rangle\rangle_{inv}$ for toluene*–SF_6 collisions determined using method *A*. Figure 2 compares the two methods over a wide range of average energies, showing general agreement in $\langle\langle \Delta E \rangle\rangle_{inv}$ at all energies, but distinct differences in the detailed shapes. The downward trend in $\langle\langle \Delta E \rangle\rangle_{inv}$ at high $\langle\langle E \rangle\rangle_{inv}$ shown in Fig. 2 is consistently observed when method *A* is used but is not present with method *B*. Although this difference is small and may not be significant, the fact that fewer assumptions are needed in method *B* leads us to prefer this approach. In addition, the uncertainties in $\langle\langle E \rangle\rangle_{inv}$ determined by error propagation in method *B* are much closer to our expectations, especially at high energies (which correspond to early times in the collisional cascade when the uncertainties should be small).

The earliest portion of the experimental IRF decay curves is dominated by the limited time response of the infrared detector. For pure toluene, tests were performed in which data prior to 4–10 μs were neglected in the least-squares curve fitting in order to determine how much of the data must be omitted in order to avoid contamination due to the slow detector rise time (because of the relatively low S/N ratio in these experiments, it was not possible to numerically deconvolute the effect of the detector rise time). It was found that after 5–6 μs, all the least-squares fits produced very similar values of the fitted parameters. All of the results reported here were obtained with data starting at $t = 7\,\mu$s. The effect of the omitted data is minimized at low pressures, where the IRF decay is slow, but the effect becomes more significant at higher pressures. By combining results obtained at pressures ranging from low to high pressures, the effect is minimized, although it still plays a role at high energy. For this reason, data above 35 000 cm^{-1} are not shown in most figures, even though the initial excitation energy was

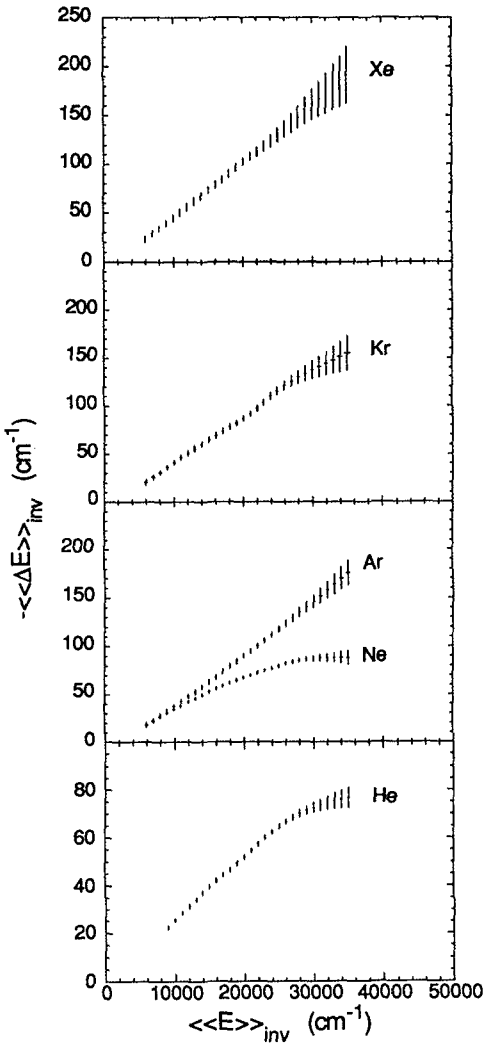

FIG. 5. – $\langle\langle \Delta E \rangle\rangle_{inv}$ vs $\langle\langle E \rangle\rangle_{inv}$ for toluene* deactivation by rare gases.

$\sim$41 000 cm^{-1}. Data below 5000 cm^{-1} are not shown, because Eq. (3) is not appropriate below that energy.

The results of the present work (analyzed according to method *B*) are presented in Figs. 2 and 4–10. In Table I, values of $\langle\langle \Delta E \rangle\rangle_{\text{inv}}$ are presented at $\langle\langle E \rangle\rangle_{\text{inv}} = 24\,000$ cm^{-1}; this energy was selected in order to allow direct comparisons with the tabulated data for azulene.[2(e)] For all collider gases investigated in this study, $\langle\langle \Delta E \rangle\rangle_{\text{inv}}$ is nearly linearly dependent on $\langle\langle E \rangle\rangle_{\text{inv}}$ at low energies, and, for most collider gases, $\langle\langle \Delta E \rangle\rangle_{\text{inv}}$ shows a tendency toward weaker energy dependence at energies above about 25 000 cm^{-1}. This behavior is most apparent for the larger colliders.

The rare gases (Fig. 5) exhibit a monotonic trend toward higher $\langle\langle \Delta E \rangle\rangle_{\text{inv}}$ values with increasing mass, similar to azulene,[2(e)] but unlike benzene.[4] The reason for this behavior is not clear, but it may be related to the magnitude of the lowest-frequency internal modes in azulene and toluene, compared to benzene. It was argued previously[4] that helium is anomalously efficient in deactivating benzene due to the relative "impulsiveness" of its collisions in deactivating the lowest-frequency mode. In toluene and azulene, the lowest-frequency modes are much lower in energy than in benzene and perhaps the impulsiveness of the collision is less important.

A similar argument may apply to the relative efficiencies of hydrogen and deuterium, where the rotational velocities of these two diatomics may be important factors.[4] For toluene deactivation, hydrogen and deuterium give values for $\langle\langle \Delta E \rangle\rangle_{\text{inv}}$ that are similar to one another: there is little

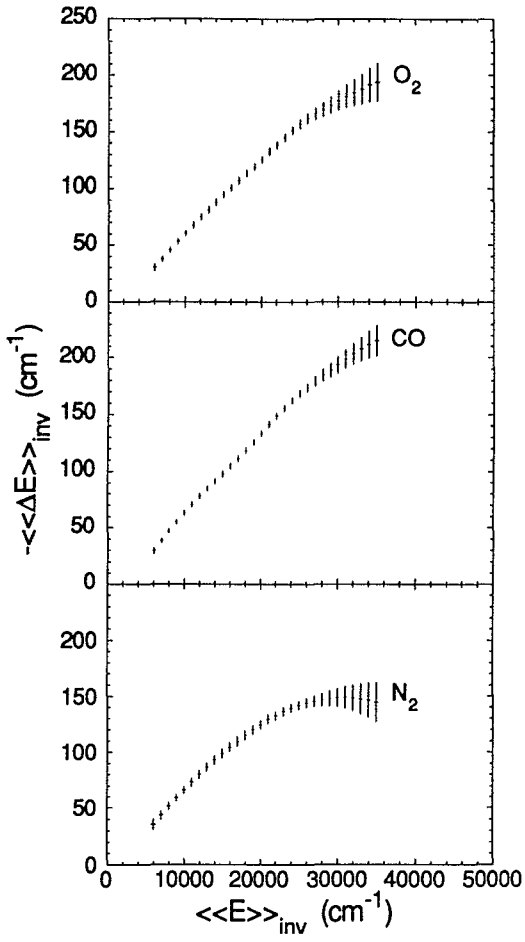

FIG. 7. — $\langle\langle \Delta E \rangle\rangle_{\text{inv}}$ vs $\langle\langle E \rangle\rangle_{\text{inv}}$ for toluene* deactivation by several diatomics.

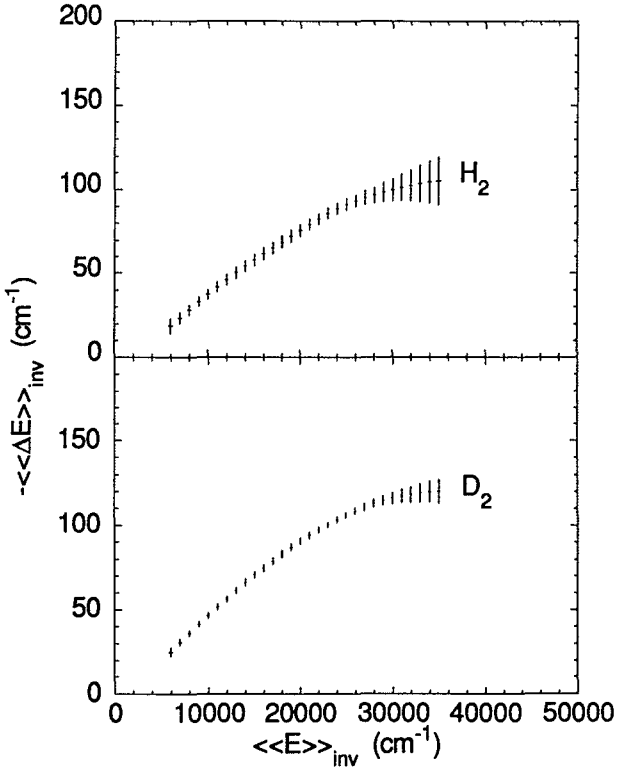

FIG. 6. — $\langle\langle \Delta E \rangle\rangle_{\text{inv}}$ vs $\langle\langle E \rangle\rangle_{\text{inv}}$ for toluene* deactivation by hydrogen and deuterium.

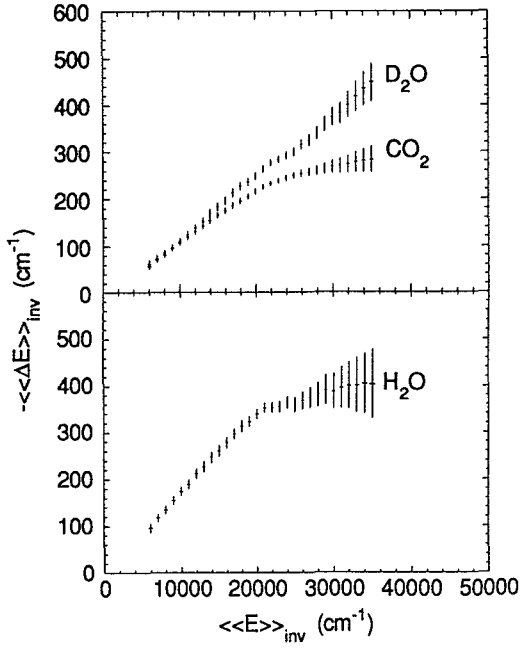

FIG. 8. — $\langle\langle \Delta E \rangle\rangle_{\text{inv}}$ vs $\langle\langle E \rangle\rangle_{\text{inv}}$ for toluene* deactivation by several triatomics.

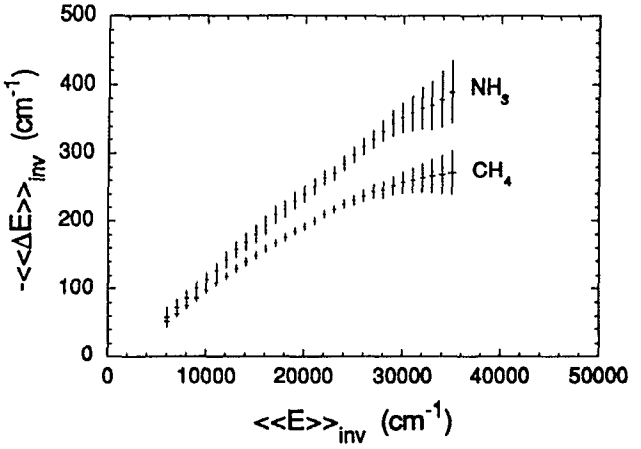

FIG. 9. – $\langle\langle \Delta E \rangle\rangle_{inv}$ vs $\langle\langle E \rangle\rangle_{inv}$ for toluene* deactivation by ammonia and methane.

isotope effect. Much more pronounced isotope effects are observed in the deactivation of benzene, where the ratio of $\langle\langle \Delta E \rangle\rangle_{inv}$ values is $\sim\sqrt{2}$, and in azulene, where the ratio is ~ 1.2. In discussing the isotope effect in benzene deactivation, it was suggested that the higher rotational velocity in H_2 favored energy transfer from the lowest-frequency modes of the excited benzene (or azulene).[4] In toluene, the lowest-frequency mode is the internal rotation and it is possible that its effective frequency is so low that the higher rotational velocity of H_2 provides no energy-transfer advantage over D_2, producing nearly equal $\langle\langle \Delta E \rangle\rangle_{inv}$ values for the two colliders. Similar arguments may apply to deactivation by H_2O and D_2O, which show only a small isotope effect.

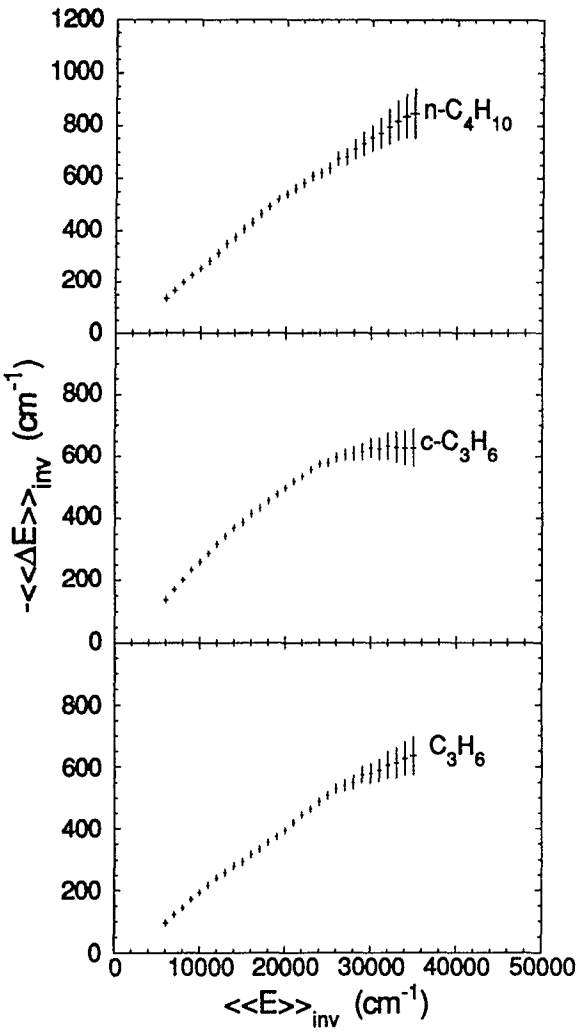

FIG. 10. – $\langle\langle \Delta E \rangle\rangle_{inv}$ vs $\langle\langle E \rangle\rangle_{inv}$ for toluene* deactivation by complex hydrocarbons.

Excited toluene, azulene,[2] and benzene[4] are all deactivated more efficiently by NH_3 than by nonpolar colliders with similar properties, such as CH_4. This effect may be due partly to an underestimate of the collision frequency, but it may also be a direct consequence of the presence of the permanent dipole moment. The permanent dipole in the collider can provide a coupling pathway that is not available to nonpolar gases. Specifically, the oscillating dipolar fields associated with the vibrational modes of the highly excited polyatomic may couple with the permanent dipole of the collider gas, opening a route for vibration–rotation energy transfer. This conjecture might be tested directly by using appropriate classical trajectory calculations.

Further speculations about the origins of the trends observed here must await development of better theoretical models. More than 20 years ago, Rabinovitch and coworkers[45] found the same qualitative trend in collider efficiency that is observed here, and it is still not explained satisfactorily.[1]

B. $\langle \Delta E \rangle_d$ from $\langle\langle \Delta E \rangle\rangle_{inv}$ data

For master-equation calculations, weak-collider unimolecular reaction calculations, and other numerical simulations of chemical systems where energy transfer plays a role, it is often most convenient to use energy-transfer data in the form of $\langle \Delta E(E) \rangle_d$, the microcanonical average energy lost in deactivation collisions as a function of the energy E. Since the IRF and UVA techniques give results in terms of bulk averages over both up and down steps and over a population energy distribution, further analysis is needed to extract $\langle \Delta E \rangle_d$. In addition to $\langle \Delta E \rangle_d$, numerical simulations also require the functional form of the collision step-size distribution function $P(E',E)$, which describes the probability that a molecule with initial energy E will have energy E' following a single collision. Because the functional form of $P(E',E)$ is not known, various assumed and calculated forms have been adopted[1,20] in numerical calculations and it has been found[1,20] that the exact functional form of $P(E',E)$ is not very important in many applications.

In the past, $\langle \Delta E \rangle_d$ has been obtained from $\langle\langle \Delta E \rangle\rangle_{inv}$ vs $\langle\langle E \rangle\rangle_{inv}$ data through laborious master-equation simulations of experiments, while utilizing assumed functional forms for $P(E',E)$.[2(a)] In this section, we describe an efficient method for obtaining estimates of $\langle \Delta E(E) \rangle_d$ [exponential model for $P(E',E)$] directly from $\langle\langle \Delta E \rangle\rangle_{inv}$ vs $\langle\langle E \rangle\rangle_{inv}$ data sets, eliminating the need for the time-consuming master-equation simulations.

The exponential model for $P(E',E)$ is well known and has been used extensively,[1,20] primarily because of its mathematical simplicity. An approximate relationship between

$\langle \Delta E \rangle_d$ and $\langle \Delta E \rangle$ (average over up and down steps) was derived previously, based on detailed balance between up and down steps and the exponential model for down steps.[2(c)] The exponential model for down steps is given by

$$P(E',E) = \exp[-(E-E')/\alpha], \quad 0 \leqslant E' \leqslant E, \tag{6}$$

where α is a parameter. For the exponential model, $\langle \Delta E \rangle_d$ is given by

$$\langle \Delta E \rangle_d = \frac{\int_0^E (E-E')P(E',E)dE'}{\int_0^E P(E',E)dE'} = \frac{\alpha - (E-\alpha)\exp(-E/\alpha)}{1-\exp(-E/\alpha)}. \tag{7}$$

Note that when α is much smaller than E, $\langle \Delta E \rangle_d \approx \alpha$. The approximate relationship between $\langle \Delta E \rangle$ and α derived earlier[2(c)] is

$$\langle \Delta E \rangle = C^{-1} - \alpha, \tag{8}$$

$$C = \alpha^{-1} + (kT)^{-1} - B. \tag{9}$$

The factor $B = d[\ln(\rho(E))]/dE$ is based on the Whitten–Rabinovitch approximation for the density of rovibrational states;[46,47] for toluene, which contains an internal rotor in addition to vibrations,

$$B = \frac{s - 1 + r/2}{E + a(E)E_z}, \tag{10}$$

where s is the number of vibrations, r is the number of rotations, E_z is the zero-point energy, and $a(E)$ is the Whitten–Rabinovitch parameter. Equation (8) for $\langle \Delta E \rangle$ has been shown to give results in excellent agreement with values obtained by numerical integration with exact densities of states both at low temperatures, where $\langle \Delta E \rangle$ is less than zero, and at high temperatures, where $\langle \Delta E \rangle$ can be greater than zero.[1(d),2(c)]

A simple approximate relationship between $\langle \Delta E \rangle_d$ and $\langle \Delta E \rangle$ is obtained from the preceding equations by assuming $\alpha = \langle \Delta E \rangle_d$; this relationship is numerically accurate, except at energies less than a few times α. Although α may be energy dependent, the dependence on energy is found experimentally to be weak and it does not significantly affect the equations above, where energy dependence was not considered. To obtain $\langle \Delta E(E) \rangle_d$ from $\langle\langle \Delta E \rangle\rangle_{\text{inv}}$ vs $\langle\langle E \rangle\rangle_{\text{inv}}$ data sets, we first neglect the effect of the bulk population distribution and assume $E \approx \langle\langle E \rangle\rangle_{\text{inv}}$ and then identify $\langle \Delta E \rangle$ with $\langle\langle \Delta E \rangle\rangle_{\text{inv}}$. The estimated $\langle \Delta E(E) \rangle_d$ is obtained by assuming it is given by a power series with coefficients that are adjusted by nonlinear least squares to give agreement between $\langle \Delta E \rangle$ calculated from the above equations and the experimental $\langle\langle \Delta E \rangle\rangle_{\text{inv}}$ values.

In the present work, excellent fits to the experimental data were obtained using $\langle \Delta E(E) \rangle_d = C_1 + C_2E + C_3E^2$; use of a higher-order polynomial did not produce better least-squares fits to the data. The nonlinear least-squares fitting was carried out using the KaleidaGraph (version 2.1, Synergy Software and Abelbeck Software) computer software, which apparently uses the Marquardt algorithm, on a Macintosh computer (Apple Computer, Inc.). The fitted values for the coefficients are collected in Table I and they provide useful functional forms for $\langle \Delta E(E) \rangle_d$. They also may be used with the above equations to reproduce accurate numerical values for all the $\langle\langle \Delta E \rangle\rangle_{\text{inv}}$ vs $\langle\langle E \rangle\rangle_{\text{inv}}$ data sets over the range of energies from 5000 to 35 000 cm^{-1} (40 000 cm^{-1} for the toluene collider). For convenience, the Whitten–Rabinovitch parameters used in the present analysis for toluene are summarized in Table II.

TABLE II. Whitten–Rabinovitch parameters for toluene.[a]

Free rotors	1
Harmonic oscillators	38
Zero-point energy	27 109 cm^{-1}
Geometric mean frequency	1171.9898 cm^{-1}
β_{vr} [b]	1.3824

[a] Vibrational assignment from Ref. 40.
[b] For rovibrational states.

Master-equation simulations were carried out to determine whether the approximate expressions for $\langle \Delta E(E) \rangle_d$ obtained above are useful for quantitative calculations. Specifically, the IRF experiments were simulated using the stochastic master-equation implementation described elsewhere,[2,4] assuming an exponential model and energy-dependent $\langle \Delta E(E) \rangle_d$ from Table I. The calculated IRF decay curves were inverted to energy decays by using Eq. (8) and $\langle\langle \Delta E \rangle\rangle_{\text{inv}}$ vs $\langle\langle E \rangle\rangle_{\text{inv}}$ data sets were generated from the derivatives of polynomial least-squares fits of $\langle\langle E \rangle\rangle_{\text{inv}}$ as a function of the number of collisions, according to Eq. (4b). Examples of the simulated $\langle\langle \Delta E \rangle\rangle_{\text{inv}}$ vs $\langle\langle E \rangle\rangle_{\text{inv}}$ data sets are plotted in Fig. 11 along with those obtained experimentally. The figure shows the agreement between simulations and experiments to be very good, although slightly better agreement might be obtained by further refinement of the parameters through master-equation simulations. Further refinements are not justified at this time, because the actual functional form of $P(E',E)$ is not yet known and it is not likely to be a simple exponential.

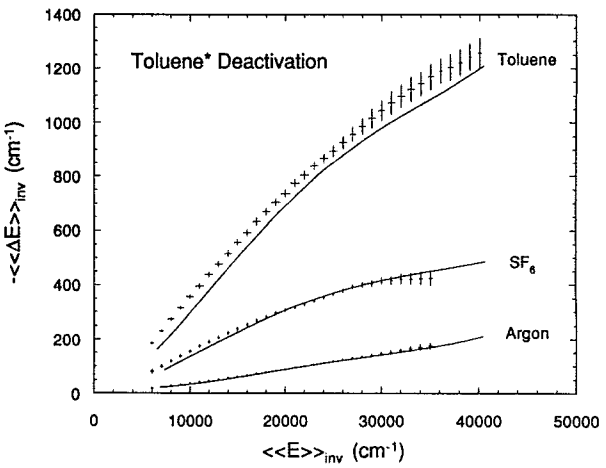

FIG. 11. Master-equation calculations compared with experimental data for $-\langle\langle \Delta E \rangle\rangle_{\text{inv}}$ vs $\langle\langle E \rangle\rangle_{\text{inv}}$ for toluene* deactivation by several gases. The calculations are based on expressions for the microcanonical $\langle \Delta E \rangle_d$ from Table I.

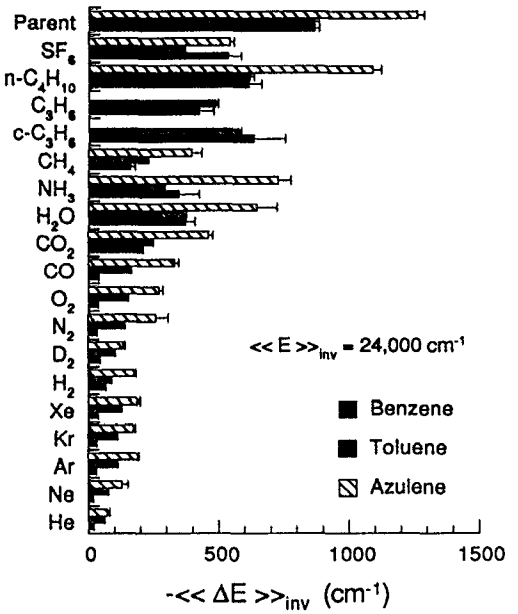

FIG. 12. Magnitudes of $-\langle\langle \Delta E \rangle\rangle_{\text{inv}}$ for azulene [Ref. 2(e)], benzene (Ref. 4), and toluene (this work) evaluated at $\langle\langle E \rangle\rangle_{\text{inv}} = 24\,000\ \text{cm}^{-1}$.

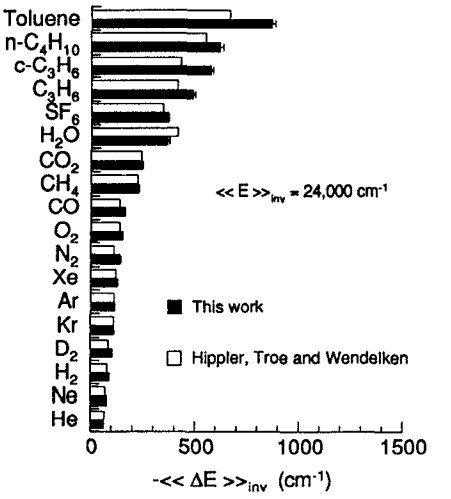

FIG. 13. Magnitudes of $-\langle\langle \Delta E \rangle\rangle_{\text{inv}}$ for toluene (this work) compared with literature values [Ref. 6(b)] evaluated at $\langle\langle E \rangle\rangle_{\text{inv}} = 24\,000\ \text{cm}^{-1}$.

However, it is noteworthy that $\langle \Delta E(E) \rangle$ for every collider gas in Table I has a tendency to roll off at higher energy. This effect is not unexpected and is reflected in the plots of $\langle\langle \Delta E \rangle\rangle_{\text{inv}}$ vs $\langle\langle E \rangle\rangle_{\text{inv}}$.

V. COMPARISON WITH OTHER RESULTS

A. IRF experiments

Previous IRF experiments on gas-phase azulene[2] and benzene[4] also show a near-linear dependence of $\langle\langle \Delta E \rangle\rangle_{\text{inv}}$ on $\langle\langle E \rangle\rangle_{\text{inv}}$ for all colliders at low energies, and in the case of benzene (analyzed by method A) a consistently weaker dependence at energies above 25 000 cm^{-1}. Figure 12 shows a comparison of $\langle\langle \Delta E \rangle\rangle_{\text{inv}}$ values for azulene, benzene, and toluene colliding with various bath gases at $\langle\langle E \rangle\rangle_{\text{inv}} = 24\,000\ \text{cm}^{-1}$. The $\langle\langle \Delta E \rangle\rangle_{\text{inv}}$ values for toluene are intermediate between azulene and benzene, but closer in value to azulene.

B. Ultraviolet absorption experiments

Collisional deactivation of toluene with an initial vibrational excitation energy of 52 000 cm^{-1} has been studied using the time-resolved ultraviolet-absorption (UVA) technique.[6(a),6(b)] This method relies on an empirical calibration curve relating the measured molecular absorption coefficient ($\lambda = 223$ nm) to the internal energy of the excited toluene. The empirical calibration curve was obtained by measuring the temperature-dependent absorption coefficient of shock-heated toluene and then assuming the thermal average absorption coefficient corresponding to an average thermal energy in the shock-heated system also corresponds to the bulk-average energy in the laser-excited energy transfer experiments. This assumption was tested with numerical simulations and with comparisons to absorption coefficients measured using laser excitation at selected wavelengths. The resulting calibration curve at 223 nm is a nearly linear function of average energy up to energies $> 52\,000\ \text{cm}^{-1}$.

For the purposes of inverting the UVA experimental data to obtain energy decay curves, the nonlinearity of the calibration curve was neglected,[6(b),6(c)] although it is quite distinct [see the figures in Ref. 6(b)]. This analysis gave $\langle\langle \Delta E \rangle\rangle_{\text{inv}}$ values nearly independent of the internal energy from $\leqslant 10\,000$ to 50 000 cm^{-1} for a large number of collider gases. Figures 13 and 14 show comparisons of the magnitudes and energy dependences of the $\langle\langle \Delta E \rangle\rangle_{\text{inv}}$ values determined in the present work and those given in Ref. 6(b) for several collider gases. The differences in energy dependence determined by the two experimental methods may arise from experimental errors, or from the neglect of the nonlinearity in the UVA empirical calibration curve. The neglect of the nonlinearity may significantly affect the derived energy dependence of $\langle\langle \Delta E \rangle\rangle_{\text{inv}}$, but the average values will be less affected. Inspection of Figs. 13 and 14 shows that the energy dependence of $\langle\langle \Delta E \rangle\rangle_{\text{inv}}$ is consistently stronger in the present IRF work than in the UVA experiments, but the magnitudes of $\langle\langle \Delta E \rangle\rangle_{\text{inv}}$ for all the collider gases are very similar at a vibrational energy of 24 000 cm^{-1} (which coincidentally falls near the intersection of the curves in Fig. 14). Thus agreement between the present results and the UVA experiments is very good despite the difference in energy dependence, which may be explained by the neglect of the nonlinearity in the UVA empirical calibration curve.

C. *P(E',E)* and "supercollisions"

In recent experiments, Luther and co-workers have used the KCSI pump-probe technique to monitor the collisional energy cascade of excited toluene (initially produced at 52 000 cm^{-1}) as it reaches an energy window at relatively low energy.[15] The KCSI experiments complement the present work, because the present work is sensitive to $\langle\langle \Delta E \rangle\rangle_{\text{inv}}$ at energies well above the bottom of the energy cascade, while the KSCI experiments monitor populations at low en-

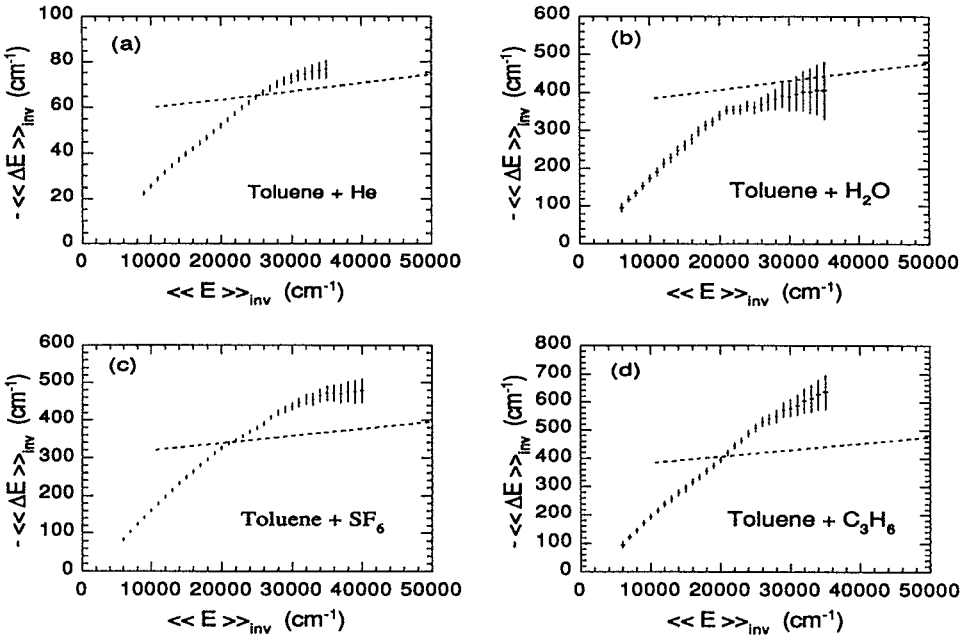

FIG. 14. $-\langle\langle \Delta E \rangle\rangle_{inv}$ vs $\langle\langle E \rangle\rangle_{inv}$ for toluene. This work: $\pm 2\sigma$ statistical error bars; literature values [Ref. 6(b)]: straight dashed lines.

ergies, where most of the cascade has already occurred. Essentially, the KCSI technique measures a quantity related to the arrival time distribution, and thus it is possible to deduce not only the average arrival time, but also the width of the population energy distribution.

When a full description of the KCSI results are available, they can be used along with the present results to obtain estimates of the functional form of the collision step-size distribution: $P(E',E)$. In modeling the KCSI results, Luther and co-workers assumed the following step-size distribution (not normalized) for down steps:[15]

$$P(E'E) = (1-f_c)\exp[-(E-E')/\alpha_1(E)] + f_c \exp[-(E-E')/\alpha_2(E)], \quad (11)$$

where $\alpha_1(E)$ and $\alpha_2(E)$ are parameters for the exponential model and f_c ranges from 0 to 1. To fit the KCSI results, $\alpha_2(E)$ was assumed by Luther and co-workers to correspond to large supercollisions. As mentioned in the Introduction, the existence of such supercollisions has been indicated in the earlier experiments of Oref and co-workers[28] and in recent calculations.[29]

To determine whether the IRF results can accommodate a contribution from supercollisions, master-equation calculations were carried out for toluene and argon collider gases in the present work. In each case, it was assumed that $\alpha_2(E) = 40\,000\ \text{cm}^{-1}$ and $\alpha_1(E)$ was equal to $\langle \Delta E(E) \rangle_d$, as tabulated in Table I for the appropriate collider gas. The fraction f_c was varied to determine the effect on the simulated IRF emission intensity decay and on the resulting plots of calculated $\langle\langle \Delta E \rangle\rangle_{inv}$ vs $\langle\langle E \rangle\rangle_{inv}$. Calculated and experimental results for toluene and for argon collider gases are compared in Fig. 15, where it is apparent that f_c(toluene) $= 10^{-3}$ and f_c(argon) $= 10^{-5}$ are not seriously inconsistent with the experimental data, but larger values of f_c produce significant discrepancies, for this choice of α_2. These values of f_c are not inconsistent with the results from the KCSI experiments. It is highly desirable to combine results from the two types of experiments to obtain better representations of $P(E',E)$. A unified treatment of the KCSI and the present experiments should be possible when the full description of the KCSI results is published.

VI. CONCLUSIONS

An important motivation for the present experiments is to establish a database of high-quality experimental results for comparisons with theoretical calculations, when they become available. The benzene derivatives were chosen for several reasons: because they are relatively small "large molecules" and therefore are tractable for theoretical calculations of large-molecule dynamics; because some information is available about their photophysical properties;

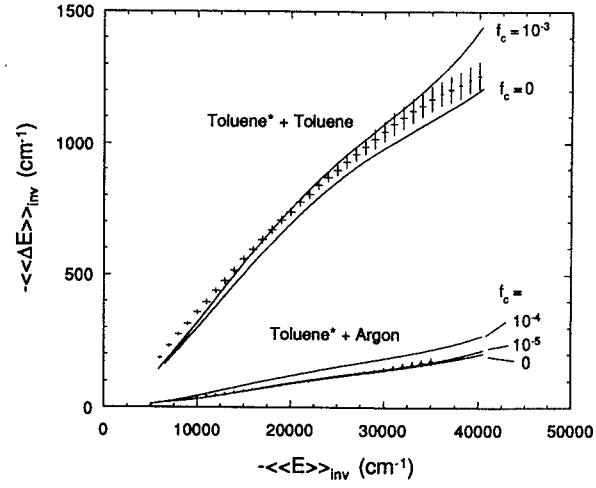

FIG. 15. Possible contributions from "supercollisions." The parameter f_c defined in Eq. (11) is a measure of the importance of supercollisions (see text for details).

and because the influence of various molecular properties can be investigated by choosing suitable derivatives. A wide variety of behavior is observed for $\langle\langle \Delta E \rangle\rangle_{\text{inv}}$, but there is little theoretical basis for its interpretation. Differences among gases are observed which cannot be explained simply and one can only speculate about the causes involved.

At present, no theoretical models are available which can provide a quantitative description of energy transfer from vibrationally highly excited large molecules, although several models can give qualitative agreement, or can be adjusted to fit the data. Trajectory calculations appear promising for modeling energy transfer involving large molecules, because the many molecular properties which may contribute effects can all be included in a single calculation. Unfortunately, accurate potential surfaces are lacking and classical statistics differ from quantum statistics in an important way,[25] leading to a fundamental problem in relating classical trajectory calculations to real experimental data.

To make progress toward a complete understanding of large-molecule energy transfer, experimental systems must be selected to investigate specific aspects of energy transfer. Results of an investigation of isotope effects in large-molecule energy transfer will be reported,[5] in which it is shown that resonance effects play no significant role in determining $\langle\langle \Delta E \rangle\rangle$ values. Also, investigations soon will be reported of energy transfer between some benzene derivatives and CO_2 in which infrared fluorescence[48] and tunable diode laser spectroscopy[30] are used to monitor V–V energy transfer; the aim is to determine the importance of V–V energy transfer in these systems and the results can be interpreted[48] to indicate that resonance effects may play a role in governing the extent of V–V energy transfer for some systems, but V–V energy transfer makes only a minor contribution to the total $\langle\langle \Delta E \rangle\rangle$.

The data in Table I and in the figures show the same general trend with molecular size and complexity found in unimolecular reaction systems and in other physical measurements of energy transfer. Discussions and rationalizations of the observed trends are not repeated here, because they can be found in previous publications by many workers.[1] Due to the lack of data concerning the step-size distribution function and the lack of suitable theoretical models, further analysis is premature and probably uninformative at this time. One of the highest priorities in studies of large-molecule energy transfer must be to elucidate the mechanisms active in large-molecule energy transfer, so that predictive theoretical models can be developed.

ACKNOWLEDGMENTS

This work was funded in part by the Department of Energy, Office of Basic Energy Sciences. K.D.K was supported in part by the U.S./Australia Bilateral Science and Technology Program. J.D.B. is grateful for a NASA graduate fellowship and W.E.C. thanks NSF for an undergraduate fellowship as part of the Research Experiences for Undergraduates program in the Department of Atmospheric, Oceanic, and Space Sciences.

[1] (a) D. C. Tardy and B. S. Rabinovitch, Chem. Rev. **77**, 369 (1977); (b) M. Quack and J. Troe, *Gas Kinetics and Energy Transfer* (Chemical Society, London, 1977), Vol. 2; (c) H. Hippler and J. Troe, in *Bimolecular Collisions*, edited by J. E. Baggott and M. N. Ashford (The Royal Society of Chemistry, London, 1989), p. 209; (d) I. Oref and D. C. Tardy, Chem. Rev. **90**, 1407 (1990).

[2] (a) M. J. Rossi, J. R. Pladziewicz, and J. R. Barker, J. Chem. Phys. **78**, 6695 (1983), and references therein; (b) J. R. Barker, J. Phys. Chem. **88**, 11 (1984); (c) J. R. Barker and R. E. Golden, *ibid.* **88**, 1012 (1984); (d) J. Shi, D. Bernfeld, and J. R. Barker, J. Chem. Phys. **88**, 6211 (1988); (e) J. Shi and J. R. Barker, *ibid.* **88**, 6219 (1988).

[3] J. M. Zellweger, T. C. Brown, and J. R. Barker, J. Chem. Phys. **83**, 6261 (1985).

[4] M. L. Yerram, J. D. Brenner, K. D. King, and J. R. Barker, J. Phys. Chem. **94**, 6341 (1990).

[5] B. M. Toselli and J. R. Barker (unpublished).

[6] (a) H. Hippler, J. Troe, and J. Wendelken, Chem. Phys. Lett. **84**, 257 (1981); (b) J. Chem. Phys. **78**, 5351 (1983); **78**, 6709 (1983); **78**, 6718 (1983); (c) **80**, 1853 (1984); (d) H. Hippler, L. Lindemann, and J. Troe, *ibid.* **83**, 3906 (1985); (e) H. Hippler, B. Otto, and J. Troe, Ber. Bunsenges, Phys. Chem. **93**, 428 (1989).

[7] N. Nakashima and K. Yoshihara, J. Chem. Phys. **77**, 6040 (1982); **79**, 2727 (1983).

[8] B. Abel, B. Herzog, H. Hippler, and J. Troe, J. Chem. Phys. **91**, 900 (1989).

[9] M. Heymann, H. Hippler, D. Nahr, H. J. Plach, and J. Troe, J. Phys. Chem. **92**, 5507 (1988).

[10] J. E. Dove, H. Hippler, and J. Troe, J. Chem. Phys. **82**, 1907 (1985); M. Heymann, H. Hippler, H. J. Plach, and J. Troe, *ibid.* **87**, 3867 (1987).

[11] For a review, see J. R. Barker and B. M. Toselli, in *Photothermal Investigations of Solids and Fluids*, edited by Jeffrey A. Sell (Academic, Boston, 1989), p.155.

[12] B. M. Toselli, T. L. Walunas, and J. R. Barker, J. Chem. Phys. **92**, 4793 (1990).

[13] T. J. Wallington, M. D. Scheer, and W. Braun, Chem. Phys. Lett. **138**, 538 (1987).

[14] K. M. Beck, A. Rengwelski, and R. J. Gordon, Chem. Phys. Lett. **121**, 529 (1985); K. M. Beck and R. J. Gordon, J. Chem. Phys. **87**, 5681 (1987).

[15] H. G. Löhmannsröben and K. Luther, Chem. Phys. Lett. **144**, 473 (1988); K. Luther and K. Reihs, Ber. Bunsenges. Phys. Chem. **92**, 442 (1988); K. Luther (private communication).

[16] T. J. Bevilacqua, B. K. Andrews, J. E. Stout, and R. B. Weisman, J. Chem. Phys. **92**, 4627 (1990).

[17] R. N. Schwartz, Z. I. Slawsky, and K. F. Herzfeld, J. Chem. Phys. **20**, 1591 (1952).

[18] F. I. Tanczos, J. Chem. Phys. **30**, 1119 (1959).

[19] J. T. Yardley, *Introduction to Molecular Energy Transfer* (Academic, New York, 1980), Chap. 4.

[20] For a recent survey, see R. G. Gilbert and S. C. Smith, *Theory of Unimolecular and Recombination Reactions* (Blackwell Scientific, Oxford, 1990), Chap. 5.

[21] H. W. Schranz and S. Nordholm, Int. J. Chem. Kinet. **13**, 1051 (1981).

[22] M. G. Sceats, J. Chem. Phys. **91**, 6795 (1989); R. G. Hynes and M. G. Sceats, *ibid.* **91**, 6804 (1989).

[23] R. G. Gilbert, J. Chem. Phys. **80**, 5501 (1984).

[24] K. F. Lim and R. G. Gilbert, J. Chem. Phys. **84**, 6129 (1986); **92**, 1819 (1990).

[25] B. M. Toselli and J. R. Barker, Chem. Phys. Lett. **174**, 304 (1990).

[26] K. F. Lim and R. G. Gilbert, J. Phys. Chem. **94**, 72 (1990); **94**, 77 (1990).

[27] M. Bruehl and G. C. Schatz, J. Chem. Phys. **89**, 770 (1988); J. Phys. Chem. **92**, 7223 (1988).

[28] S. Hassoon, I. Oref, and C. Steel, J. Chem. Phys. **89**, 1743 (1988); I. M. Morgulis, S. S. Sapers, C. Steel, and I. Oref, *ibid.* **90**, 923 (1989); A. Pashutzki and I. Oref, J. Phys. Chem. **92**, 178 (1988).

[29] G. Lendvay and G. C. Schatz, J. Phys. Chem. **94**, 8864 (1990).

[30] A. J. Sedlacek, R. E. Weston, Jr., and G. W. Flynn, J. Chem. Phys. (in press); and (personal communication).

[31] C. S. Burton and W. A. Noyes, J. Chem. Phys. **49**, 1705 (1968).

[32] L. D. Brouwer, W. Müller-Markgraf, and J. Troe, J. Phys. Chem. **92**, 4905 (1988).

[33] T. G. Dietz, M. A. Duncan, and R. E. Smalley, J. Chem. Phys. **76**, 1127 (1982).

[34] J. B. Birks, *Organic Molecular Photophysics* (Wiley, London, 1975), Vol. 2.

[35] M. Jacon, C. Lardeux, R. Lopez-Delgado, and A. Tramer, Chem. Phys. **24**, 145 (1977).
[36] C. E. Otis, J. L. Knee, and P. M. Johnson, J. Phys. Chem. **87**, 2232 (1983).
[37] H. G. Lömannsröben, K. Luther, and M. Stuke, J. Phys. Chem. **91**, 3499 (1987).
[38] P. R. Bevington, *Data Reduction and Error Analysis for the Physical Sciences* (McGraw-Hill, New York, 1969), p. 237.
[39] J. F. Durana and J. D. McDonald, J. Chem. Phys. **64**, 2518 (1976).
[40] J. A. Draeger, Spectrochim. Acta **41**, 607 (1985); H. D. Rudolph, H. Dreizler, A. Jauschke, and P. Wendling, Z. Naturforsch. **22**, 940 (1967).
[41] S. E. Stein and B. S. Rabinovitch, J. Chem. Phys. **58**, 2438 (1973).
[42] T. Beyer and D. F. Swinehart, Commun. ACM **16**, 379 (1973).
[43] D. C. Astholz, J. Troe, and W. Wieters, J. Chem. Phys. **70**, 5107 (1979).
[44] A. P. Penner and W. Forst, J. Chem. Phys. **67**, 5296 (1977).
[45] Y. N. Lin, S. C. Chan, and B. S. Rabinovich, J. Phys. Chem. **72**, 1932 (1968).
[46] G. Z. Whitten and B. S. Rabinovitch, J. Chem. Phys. **41**, 1883 (1964).
[47] W. Forst, *Theory of Unimolecular Reactions* (Academic, New York, 1973).
[48] B. M. Toselli and J. R. Barker (unpublished).